International Journal of Thermal Sciences 225 (2026) 110749

Contents lists available at ScienceDirect

International Journal of Thermal Sciences

journal homepage: www.elsevier.com/locate/ijts

A numerical study on cryogenic sprays under different break-up regimes

Mattia Pelosin [a,*], Francesco Duronio [d,g], Paolo Albertelli [a,b], Tommaso Lucchini [c], Zhifu Zhou [e], Jiameng Tian [f], Bin Chen [e]

[a] Politecnico di Milano, Department of Mechanical Engineering, via La Masa, 1, Milan, 20156, Lombardy, Italy
[b] MUSP Macchine Utensili Sistemi di Produzione, strada della Torre della Razza, Piacenza, 29122, Emilia-Romagna, Italy
[c] Politecnico di Milano, Department of Energy, via Lambruschini, 4, Milan, 20156, Lombardy, Italy
[d] Università degli studi dell' Aquila, Piazzale Ernesto Pontieri, Aquila, 67100, Abruzzo, Italy
[e] State Key Laboratory of Multiphase Flow in Power Engineering, Xi'an Jiaotong University, Xi'an, 710049, China
[f] School of Energy and Power Engineering, Jiangsu University, Zhenjiang, 212013, China
[g] Institute of Sciences and Technologies for Sustainable Energy and Mobility (STEMS) - National Research Council, Via G. Marconi 4, Napoli, 80125, Italy

ARTICLE INFO

Keywords:
Cryogenic spray
Lagrangian spray
Flash boiling numerical modeling

ABSTRACT

CFD simulation of cryogenic sprays represents a challenging task that requires an accurate modeling of the specific thermodynamic-induced primary break-up and evaporation rate. This work presents a computational approach based on the Eulerian–Lagrangian framework to simulate cryogenic flashing sprays. Dedicated models are included to account for flash boiling in atomization, nozzle flow and phase change processes, removing the need to tune conventional break-up models to describe the spray evolution when flash boiling atomizing takes place. The proposed methodology is validated using experimental measurements of local spray properties (velocity, droplet diameter and temperature). The proposed model accurately captures the characteristics of the different breakup regimes (mechanical, transient and fully flashing break-up) reproducing experimental data both in terms of spray morphology and the thermophysical evolution of the vapor and liquid phases.

1. Introduction

In the context of the energy transition, various cryogenic spray systems are gaining increasing importance for fuel injection and cooling applications. Liquid hydrogen (LH_2) and liquid methane (LCH_4) are promising propellants in the aerospace field, due to the eco-friendly and high energy density characteristics [1]; in the same field liquid oxygen (LO_2) is also used as an oxidizer. In the manufacturing sector, the replacement of oil-based lubricants with cryogenic fluids in the cutting technologies improves the process's overall performance, especially for hard-to-cut materials, such as titanium alloys [2]. Furthermore, flashing spray cooling with cryogen R134a is widely used in cutaneous laser surgeries [3]. Cryogenic liquids are substances that exist as gases under ambient conditions, since their saturation pressure exceeds the ambient one. To maintain them in the liquid phase, they are typically stored in pressurized, thermally insulated tanks (dewars) under saturated conditions. When they are injected in ambient-like conditions, the liquid pressure drops suddenly, causing the nucleation, growth and expansion of vapor bubbles [4]. Beyond fast vaporization, this can lead to the liquid breaking apart into tiny droplets, which significantly affects the spray morphology [5]. This thermodynamically driven break-up takes the name of flash boiling and, compared to spray formation through conventional methods, produces droplets with a smaller average diameter, greater uniformity, and wider cone angle [6]. These features are relevant for different applications since both the cooling potential and the combustion are directly affected by the spray morphology [7]. Furthermore, flash boiling enables the creation of the desired spray characteristics at reduced injection pressures [8].

The intensity of flashing atomization is directly related to the difference between injection and ambient pressure, the greater the difference, the more intense the flashing breakup and changes in the spray morphology. Different classification methods were proposed to classify the spray characteristics on the basis of the operating conditions [5,9,10]. Among them, Cleary et al. [11] introduced modified Jakob and Weber number to identify different flashing regimes.

Optical techniques, including x-ray diagnostics, have been widely used to investigate the internal and near-nozzle flow of flashing sprays in various application fields [12,13].

From a modeling point of view, two approaches can be used to investigate this kind of multi-phase flow. The first method adopts a purely Eulerian approach, which accurately describes the liquid and gas/vapor

* Corresponding author.
E-mail addresses: mattia.pelosin@polimi.it (M. Pelosin), francesco.duronio@univaq.it (F. Duronio), paolo.albertelli@polimi.it (P. Albertelli), tommaso.lucchini@polimi.it (T. Lucchini), zfzhou@mail.xjtu.edu.cn (Z. Zhou), tianjiameng@ujs.edu.cn (J. Tian), chenbin@xjtu.edu.cn (B. Chen).

https://doi.org/10.1016/j.ijthermalsci.2026.110749
Received 4 July 2025; Received in revised form 16 December 2025; Accepted 2 February 2026
Available online 5 February 2026
1290-0729/© 2026 The Authors. Published by Elsevier Masson SAS. This is an open access article under the CC BY license (http://creativecommons.org/licenses/by/4.0/).

phases by capturing the effects responsible for the spray collapse, such as flow expansion, air entrainment and generation of low-pressure zones [14–16]. However, industrial simulations relevant for the energy transition context involve complex geometries and length-scales that are extremely large compared to the evolution of the liquid-vapor interface of a liquid droplet under flash-evaporation conditions. This calls for applying a reduced order modeling strategy that uses some simplifying hypotheses like the Eulerian-Lagrangian approach, where the liquid droplets are tracked as particles interacting with the gas phase, which is treated in an Eulerian fashion.

The Eulerian-Lagrangian approach relies on consolidated sub-models to describe the atomization and break-up processes. Nevertheless, dedicated developments and investigations are needed to predict spray break-up and phase change under flash evaporation conditions, where bubble formation inside the liquid jet promotes flash boiling break-up. Aerodynamic-based breakup models [17,18] do not account for the thermodynamic evolution of the bubble within the droplet and, therefore, cannot accurately reproduce flash-boiling phenomena without substantial tuning of model constants [19]. Although such tuning can yield satisfactory results for particular cases, it reduces the general applicability and physical consistency of the modeling framework. Another approach to account for the flashing atomization process is to employ experimental based correlations to estimate the post-atomization droplet size of flashing spray under different super-heat degree, as proposed by Wang et al. [20]. However, previous literature demonstrates how adopting an flash boiling break-up model, specifically designed to account for bubble expansion within droplets in flash-boiling sprays, significantly improves Lagrangian spray simulations. The most common approach is based on the resolution of the Rayleigh-Plesset equation for the estimation of the growth of the inner bubble, as presented by Duronio et al. [21] and similarly by Saha et al. [22]. The two approaches mainly differ in the number of growing bubbles considered.

The present work introduces a simulation methodology for cryogenic sprays in the Eulerian-Lagrangian framework. The key innovation lies in considering the breakup as being driven not only by aerodynamic forces but also by a physical-grounded flash boiling mechanism based on the modeling of the growing vapor bubble dynamics, which accounts for flash-boiling atomization. This analysis is one of the few numerical contributions in the literature on a cryogenic spray system widely used in different industrial and medical applications for cooling purposes, whose development could benefit from an accurate modeling technique. Since the thermodynamic state of the spray droplets directly affects the cooling efficiency [23,24], an accurate numerical simulation is important for the optimization of this technology. While most of the literature focuses on the fully developed flashing regime, this study also numerically investigates the transitional phase between aero-driven and flashing breakup by varying the injection parameters. This sensitivity analysis is particularly relevant, as the proposed flashing break-up model is physically guided by the dynamics of vapor bubble growth within the droplets. Consequently, the model sensitivity arises directly from the underlying physical mechanisms of flash boiling, rather than from the use of experimentally derived correlations for the post-atomization droplet diameter based on the droplet superheat degree [25], as previously proposed in the literature [20]. This analysis demonstrates the robustness and generality of the proposed simulation methodology, as cryogenic sprays involve species with markedly different physical properties and thus span a wide range of operating conditions. Consequently, a reliable simulation approach must be capable of accurately capturing variations in spray morphology across different spray systems. Furthermore, this application is characterized by low injection pressure and large nozzle diameter, resulting in a different aerodynamic regime than the majority of the research on flashing spray systems.

The proposed approach was implemented by the authors in OpenFOAM, an open-source CFD software [26] and validated with experiments carried out for a R134a cryogenic spray at atmospheric conditions [27]. The very detailed spray characterization includes measurements of local velocity, droplet diameter and temperature, allowing an extensive assessment of the simulation results.

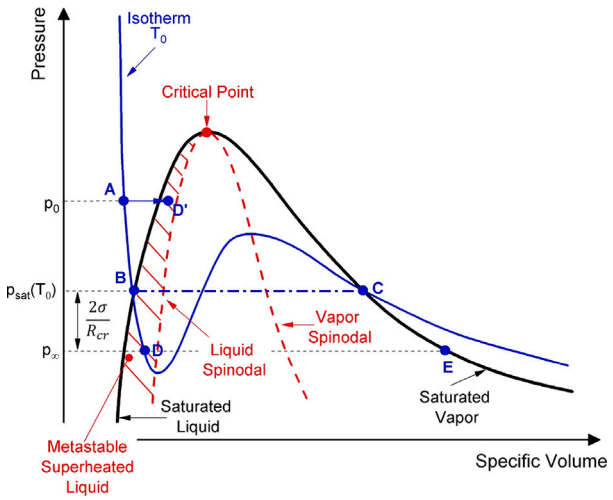

Fig. 1. p-v diagram for iso-thermal and isobaric transformation of a phase changing fluid.
Source: Reproduced with permission from Duronio et al. [28].

2. Flash boiling regime

Flashing atomization of a droplet is the result of nucleation, growth and bursting of vapor bubbles inside it. With reference to Fig. 1, when the super-heated liquid exits from the nozzle, it reaches an environment below its saturation pressure. A fast isothermal transformation occurs, bringing the liquid from a sub-cooled (A) to a super-heated state (D). Super-heat condition is metastable, hence the liquid can remain in this thermophysical state until a pressure fluctuation triggers the phase change (nucleation). The phase change (growth) lasts till the liquid is brought to stable saturated condition (E). The liquid film is characterized by a temperature larger than the vapor bubble and by a lower pressure. When the bubble exceeds a characteristic dimension, the instabilities lead to the breakage of the liquid film (burst of the droplet).

At the same time, aerodynamic forces are exchanged on the external surface of the droplet, establishing the well-known Kelvin–Helmholtz and Rayleigh–Taylor instabilities, which are responsible for the mechanical break-up. Depending on the characteristic time of these competing mechanisms different spray regimes are identified. If the aerodynamic break-up is faster than flash-boiling, the classical mechanical break-up occurs. Conversely, full-flashing regime takes place. A transition regime exists when the characteristic times of the two processes are comparable, here the bubbles alter the evolution of the spray, leading to an intermediate evolution of the spray.

This work aims to assess the sensitivity of the developed numerical methodology for cryogenic sprays at varying of the flashing regime. In order to define the operating conditions for this analysis, the authors rely on the classification of the break-up regimes proposed by Cleary et al. [11], which is based on the spray global non-dimensional parameters. The intensity of the flash boiling is controlled by the bubble growth rate, which is related to the modified Jakob number [29]:

$$Ja = \frac{C_{p,l}(T_{l,0} - T_{sat,0})}{h_{lv}} \frac{\rho_{l,0}}{\rho_v}. \quad (1)$$

This parameter is proportional to the ratio among the heat capacity of the liquid in super-heated state and the latent heat of evaporation. In

contrast, the intensity of aerodynamic break-up is proportional to the vapor Weber number:

$$We_v = \frac{d_n \rho_v u_0^2}{\sigma}, \tag{2}$$

since it is the ratio of aerodynamic and surface tension forces. Here, d_n is the diameter of the nozzle, u_0 the discharge velocity, and σ the surface tension. Both these parameters are computed at injection condition. Two experimentally derived thresholds, A and B, are proposed by Cleary et al. [11] for the transition from aerodynamic to flash boiling regime:

$$\begin{aligned} A &: Ja\Phi = 55We_v^{-1/7}, \\ B &: Ja\Phi = 150We_v^{-1/7}. \end{aligned} \tag{3}$$

where $\Phi = 1 - \exp\left(-2300\rho_v/\rho_l\right)$ is a correction factor to account for the obstruction to the bubble growth rate deriving by the simultaneous growth of different clusters of bubbles. Above the lower limit (A in Eq. (3)), the macroscopic bubbles alter the evolution of the spray, the upper (B) one marks the passage to a full flashing spray.

3. Numerical methodology

The model was implemented within the OpenFOAM® framework in a dedicated library developed by the authors. The code relies on the Eulerian-Lagrangian approach, meaning that the disperse phase (spray) is represented by a set of non-dimensional marker points (*parcels*) that are tracked in the continuous domain according to the implemented physics. The interaction with the continuous phase is obtained by specific source terms in the transport equations accounting for the parcels evolution and corresponding exchange of mass, momentum and energy. Since the droplets are not directly solved but modeled, this approach does not require an extremely refined mesh. The simulations are therefore suitable for an industrial context. Turbulence is treated in RANS fashion and the well known k-ε model was employed [30,31].

Eulerian-Lagrangian modeling is based on the definition of sub-models to account for the phenomena that cannot be directly solved, as droplet break-up and evaporation rate. For its nature, flash-boiling has a direct effect both on the dynamic evolution of the droplets (break-up) and the thermal evolution (boiling). Although these aspects are strongly coupled, they are treated separately through two distinct models: a flashing break-up model, which governs only the change in droplet diameter, and a boiling phase-change model, which accounts for the droplet's phase change. This choice is justified by the consideration that the effect of flash boiling on phase change extends far beyond the presence of a growing vapor bubble [32], but includes complex thermodynamic phenomena that cannot be captured within the framework of the break-up model. Droplets are hence initialized as fully liquid at the nozzle exit, with properties corresponding to the nozzle tip conditions. The main limitation of the Eulerian-Lagrangian approach lies in the near-nozzle region, where it cannot fully capture the complex phenomena characteristic of under-expanded two-phase jets [33]. These phenomena can be resolved through detailed Eulerian-Eulerian simulations; however, such an approach is not feasible for full spray modeling, as it would require extremely high spatial resolution over a large computational domain, making it prohibitively expensive.

3.1. Break-up models

The proposed methodology considers the break-up as a phenomenon ruled by two mechanisms: flash boiling and aerodynamic. Both models are executed concurrently throughout the simulation. The flash-boiling breakup mechanism becomes active only when the droplet saturation pressure exceeds the ambient cell pressure, as bubble growth is inhibited under subcooled conditions. Although the models operate in parallel, flashing atomization directly influences the aerodynamic breakup model. When flash boiling occurs, the droplets experience a drastic reduction in diameter. Since the governing parameter for aerodynamic breakup is the Weber number, regardless of the specific model, a drastic decrease in the droplet diameter close to the nozzle, as typical of flash-boiling, leads to a proportional decrease in the Weber number. Consequently, aerodynamic breakup is inhibited.

3.1.1. Flash boiling break-up

To implement the flash boiling break-up in a Lagrangian framework, it is necessary to predict the nucleation, growth and burst of vapor-bubbles inside the droplets, till the instant when their dimensions cause the break-up of the liquid and thus the creation of secondary droplets (Fig. 2). This model assumes the presence of a single growing bubble within each droplet. This simplification is motivated by the inherent complexity of nucleation, which makes it challenging to predict the number of bubbles formed accurately. The bubble is imagined growing inside the droplet, based on the Rayleigh equation:

$$R_i \ddot{R}_i + \frac{3}{2}\left(\dot{R}_i\right)^2 = \frac{1}{\rho_l}\left[p_v(T_v) - p_\infty\right], \tag{4}$$

in which $R_i, \dot{R}_i, \ddot{R}_i$ are respectively the bubble radius and its first and second derivatives, ρ_l is the liquid density and μ is the dynamic viscosity. p_v the saturated vapor pressure, and T_v the vapor temperature, which is assumed to be equal to the liquid temperature at the bubble surface. Since the droplet considered in this study is much larger than the bubble, it is assumed that p_∞ is the same as the surrounding gas pressure. The left-hand side of the equation represents the inertial effects, while $[p_v(T_v) - p_\infty]$ denotes the pressure differential at the liquid-vapor interface, which is the driving force for the bubble growth. The break-up model, for definition, acts only to change the droplet diameter; hence, the bubble sub-model does not effectively introduce a vapor fraction inside the droplet, but it is only used to predict the droplet break-up. The bubble radius at the instant of nucleation $R_{i,0}$ is calculated assuming an initial condition of static equilibrium ($\dot{R}_i = 0$), in which the liquid surface tension (σ) is balanced by the pressure difference at the interface Eq. (5):

$$R_{i,0} = \frac{2\sigma}{p_v(T_0) - p_\infty}, \tag{5}$$

where p_v is the liquid vapor pressure at initial temperature and p_∞ is the ambient pressure computed in the Eulerian framework, hence the pressure of the gaseous phase in the cell where the Lagrangian parcel is located. Vapor bubbles with a smaller radius cannot be formed because they collapse under the force of the surface tension. Any pressure variation will cause the bubble to grow or collapse, and for this reason, it is called the critical radius. Solving the Rayleigh equation, the bubble growth rate can be expressed as:

$$V_i = \sqrt{\frac{3}{\rho_l}\left(p_{sat} - p_\infty\right)}. \tag{6}$$

Flash boiling break-up is a consequence of the instabilities that grow on the droplet and bubble surfaces and, as discussed, are thermodynamically driven (Fig. 2-a). The instability growth rate (ω) is the largest real root of the normalized growth rate equation [21].

The droplet growth rate (V_0) can be expressed as a function of the bubble growth rate as follows [28]:

$$V_o = V_i \cdot \Delta^2, \tag{7}$$

where Δ is the ratio between the droplet and bubble radius. The temporal evolution of the instability in the liquid film, called η, growing with the rate ω, is given by the following relation:

$$\ln\left(\frac{\eta}{\eta_0}\right) = \int_0^t \omega dt. \tag{8}$$

The break-up occurs when the instability amplitude grows larger than a characteristic length of the spray (Fig. 2-b), which can be chosen as the film thickness, to be intended as the difference between droplet and bubble radius.

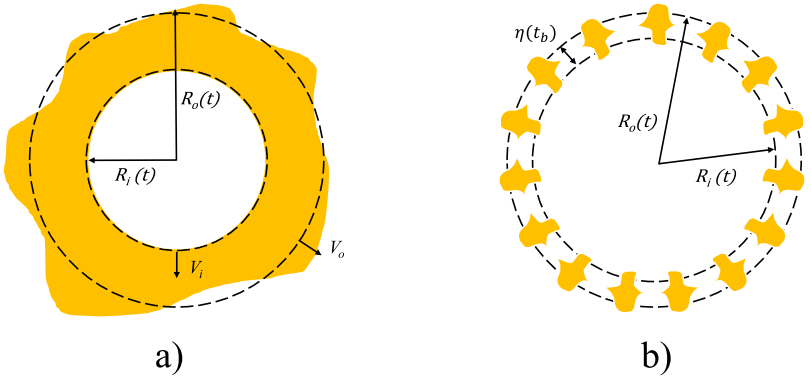

Fig. 2. Time evolution of bubble–droplet system [21].

A break-up criterion for bubble-droplet systems can be expressed a follows:

$$\frac{\eta_0 e^{\int_0^t \omega dt}}{R_o(t) - R_i(t)} = k_b(t), \tag{9}$$

assuming the initial disturbance η_0 proportional to the initial droplet radius. After a time t_b, when the instability amplitude equals the film thickness $\left(k_b\left(t_b\right) = \bar{k}_b = 1\right)$, break-up occurs. $\bar{k}_b$ is a potential parameter for model atomization to take into account the complexities found in real bubble-droplet systems. The new Sauter mean radius of the droplets (SMD) is expressed as follows:

$$SMD^{-1} = \frac{R_0^2 + R_i^2}{R_o^3 - R_i^3} + \left(\frac{3}{2}\frac{R_i^4\left(R_i^{-1} - R_o^{-1}\right)}{R_o^3 - R_i^3}V_i^2 - \frac{U_r^2}{2}\right)\frac{2\rho_\ell}{3\sigma} \tag{10}$$

and derives from the conservation of mass and energy. Since the evaporation related to lash-boiling is not accounted in the break-up model, the number of particles in a parcel (computational element in the Lagrangian approach) after the break-up is computed to ensure mass conservation:

$$n_{new}d_{new}^3 = n_{old}d_{old}^3, \tag{11}$$

where n_{new} and n_{old} are the number of particles in the current parcel after and before the break-up process. This break-up model has already been validated in previous works for fuel sprays [21,28].

3.1.2. Aerodynamic break-up

The other class of break-up models is the aerodynamic one. Within this implementation, any available aerodynamic break-up model can be used to model mainly secondary break-up processes. Since the near-nozzle spray evolution is highly affected by flashing mechanisms, the authors choose to mainly use aerodynamic models that handle the secondary break-up, hence the one that happens far from the nozzle when the primary atomization of the liquid jet has already occurred. For this reason, the well-known Pilch-Erdman model was used [34], which identifies different break-up regimes for the droplets depending on the Weber number. No tuning of break-up coefficients with respect to authors' indications is performed.

3.2. Superheated phase change model

Phase change in superheated state is the result both of the vaporization due to the heat transfer with the surrounding gas and by the specific flash vaporization. The latter contribution is mainly controlled by the available superheat energy near the droplet surface, similar to sheet flash boiling. Depending on the degree of superheat, different complex phenomena occur, which make it difficult to derive a detailed lumped model usable in the Lagrangian framework. The two contributions to the total mass transfer rate ($G = dm_d/dt$) are in competition, since the flow of boiled fuel vapor balances the heat transfer process, reducing the second contribution. The model proposed by Zuo et al. [35] (Eq. (12)) for this specific regime accounts for this competing mechanism in a non-linear implicit equation for the total mass transfer rate:

$$G = 4r_0\pi\frac{k}{C_p}\frac{Nu}{1 + G_f/G}ln\left[1 + \left(1 + \frac{G_f}{G}\right)\frac{h_\infty - h_b}{\Delta h}\right]. \tag{12}$$

where h_∞ and h_b are the gas enthalpy in the mixture and at the drop surface, respectively. Nu is the Nusselt number and r_0 is the droplet radius, k and C_p are the gaseous thermal conductivity and specific heat. The flashing contribution to the mass transfer rate ($G_f = dm_{df}/t$) is modeled by Adachi [32] as follows:

$$G_f = \frac{\alpha_s(T_l - T_{sat})A}{\Delta h}, \qquad \alpha_s = C(T_l - T_{sat})^f. \tag{13}$$

where A is the droplet surface area, T_l the liquid temperature, T_{sat} the liquid saturation pressure and Δh is the latent heat of vaporization. α_s is the overall heat transfer coefficient from the droplet interior to the droplet surface, which avoids modeling the complex physics via two experimentally derived coefficients (C and f) depending on the superheat degree. Note that this model requires an iterative resolution since Eq. (12) is implicit.

4. Test case description and simulation set-up

This section describes the spray system [27] simulated in this work, with a brief description of the measuring techniques used. The case is classified according to the methodology discussed in Section 2, and the simulation campaign conceived for the sensitivity analysis is presented. Finally, the simulation set-up is proposed.

4.1. R134a spray: experimental injection conditions and measurements

The investigated case deals with a cryogenic injection of R134a. The liquid is stored at saturated conditions in a tank at 0.7 MPa and room temperature (T = 300 K). The injector nozzle has a 63.5 mm length and 0.81 mm inner diameter. The measured liquid steady-state volume flow rate of liquid was 3.15 cm^3/s, corresponding to 3.8 g/s mass flow rate. The droplet count number, velocity and diameter were sampled with a Phase Droplet Particle Analyzer along the radial direction at four nozzle distances (50, 90, 130, 170 mm). The same procedure was conducted for the temperature measurements, performed with a thermocouple. In this case, the sampling axial positions were 10, 30, 50 and 100 mm. Spray morphology images were captured via a high-speed camera.

Fig. 3 shows the break-up regimes of the analyzed injection conditions according to the classification proposed for flashing spray. This preliminary analysis is useful since the analogy superheated fuel-flashing regime depends on the specific injection conditions. The modified Jakob number of the analyzed case (black square marker) is 121,

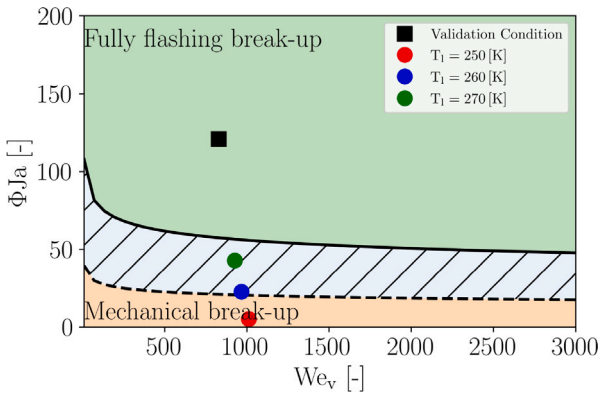

Fig. 3. Spray conditions of analyzed cases classified on the basis of Cleary [11] Break-up regimes. Circle markers represent the sweep of Ja by changing injection temperature, square marker is the case used for validation.

Table 1
Simulated conditions operating parameters, first one is the validation case, others are the sensitivity analysis.

ΦJa	p_{inj} [MPa]	T_{inj} [K]	p_{amb} [MPa]
121	0.7	300	0.1
43	0.7	270	0.1
22	0.7	260	0.1
5	0.7	250	0.1

and it is well above the full-flashing limit for its corresponding vapor Weber number. The dominant mechanism of atomization is hence flash-boiling.

4.2. Sensitivity analysis

A sweep of spray operating conditions is performed to test the model's robustness varying the break-up regimes. The change of the Jakob number is achieved by changing the injection temperature and hence the temperature at which the parcels are initialized in the computational domain. Since this dimensionless number decreases with temperature and the validation case is in fully flashing regime, the injection temperatures are selected to move from fully-developed flashing to mechanical break-up, crossing the transient regime. The range chosen varies from the validation case condition (300 K) to 250 K with two additional steps (270 K and 260 K). The bottom temperature has been chosen to investigate the mechanical break-up regime, even if it is larger than the saturation temperature at ambient pressure (211 K). All the cases operating conditions are summarized in Table 1. A small change in the vapor Weber number is also present in this sweep, since the surface tension is a function of the liquid temperature. The authors chose to move in the regimes by altering the injection temperature instead of the ambient pressure to keep the variation of the Weber number limited and therefore to isolate the effect of flash atomization. Another possibility to perform a similar analysis would be to vary the ambient pressure; however, this method would also affect the injection velocity and thus the Weber number. Except for the initial droplet temperature, all other simulation parameters remain unchanged between the cases. Therefore, the observed differences can be attributed to the sensitivity of the vapor bubble growth rate, predicted by the flashing break-up model, and to the intensity of the phase change predicted by the boiling evaporation model.

4.3. Simulation set-up

The setup of the simulation for this case consisted of a cuboid (20 × 20 × 300 mm) representing a quarter of the spray. This choice was guided by the possibility of exploiting the geometric symmetry to reduce the computational cost and to employ perfect Cartesian cells, minimizing also the mesh non-orthogonality. Since the spray is injected in an open environment, all the boundary conditions were set imposing the total pressure equal to the ambient pressure (1 bar) and a zero gradient condition for the velocity. The base mesh consists of cubic cells of side 0.8 mm. A refinement cylindrical region (10 mm radius; 70 mm height, 0.4 mm cell size) centered on the injection position was placed to simulate accurately the near-nozzle flow field.

It was noticed by the authors that the cell size in the vicinity of the injection position must be close to the nozzle diameter to capture correctly the evolution of the spray. This is justified by the importance of the interaction with the Eulerian field during the initial evolution of the droplets. A coarser mesh would not be able to capture the local variation of the turbulent flow field, producing a non-accurate evolution of the spray. This refinement constraint is even more important for flash boiling since the break-up occurs very close to the nozzle. The total number of cells is 300'000. For what concerns the numerical set-up, PIMPLE resolution algorithm has been used, with two internal pressure correctors and two outer correctors. Euler implicit time scheme was used for time discretization and secondary order limited schemes are used for divergence and Laplacian discretizations. The injected plume cone angle was set equal to 50 degrees. The simulations where carried employing a fixed maximum Courant Number, which was set equal to 0.7, in the steady state phase of the simulation this equal a time-step close to $3 \cdot 10^{-6}$ s. The parcel per second number employed is $5 \cdot 10^{6}$. Since a single-hole nozzle is analyzed and the injection velocity is relatively low, droplet–droplet interactions are expected to be limited, as the parcels tend to diverge during the spray evolution. Therefore, no collision model is applied. A value of $k_p = 1.05$ was used for all simulations, requiring only limited tuning to obtain a realistic spray behavior. A discharge coefficient (C_d) equal to 0.1 was set. The presence of a valve in the discharge system causes some internal flash-boiling. The mass flow rate is measured upstream of it, hence, for continuity, the velocity downstream is higher and it justifies the use of a smaller discharge coefficient. An initial droplet diameter equal to half of the nozzle diameter was initialized to be consistent with this choice. Moreover, it is well known [36] that cavitation is present in high-pressure nozzle. Since both cavitation and internal flash-boiling are driven by a drop of pressure in the fluid discharge system, internal flash-boiling is a common phenomenon for the super-heated spray. This statement is justified by experimental measurements of discharge coefficients for cryogenic nitrogen spray [37], ranging between 0.1 and 0.3 depending on the conditions. These values are not far from the ones used in the analyzed case.

A constant injection rate profile has been used since the measurements were carried on when the spray reached steady-state conditions. Primary atomization is guided by flash-boiling, hence the flashing break-up is faster than the mechanical one. Euler and second-order limited schemes were used for time and convection discretization, respectively. The thermodynamic properties of liquid R134a have been implemented in OpenFOAM by the authors based on the CoolProp database [38].

5. Results and discussion

This section proposes the results of the simulation campaign. The validation case is first presented: the simulated spray morphology is compared to the experimental image, and the evolution of the droplet thermophysical properties is validated. A sensitivity analysis is performed to evaluate the model validity under varying operating conditions. The focus is on the spray evolution in terms of morphology, droplet diameter, temperature, evaporation and gaseous phase temperature. These properties are chosen since they both affect the cooling characteristics of cryogenic sprays and thus cover the majority of the applications of cryogenic injections.

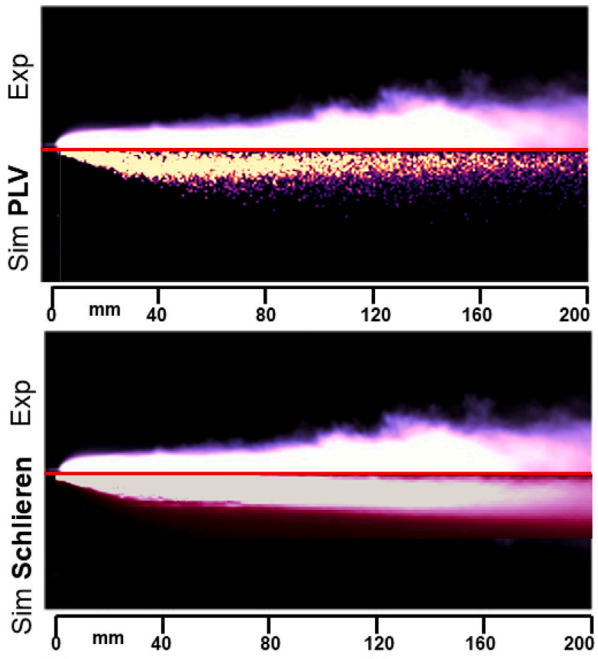

Fig. 4. Comparison between numerical simulation and experimental spray photography. Experimental image adapted from [27]. Simulation post-processing: upper panel shows Projected Liquid Volume (PLV); lower panel shows two-dimensional slices of density gradient magnitude.

5.1. Validation case

An initial qualitative assessment of the spray morphology is shown in Fig. 4. The experimental spray photographs were captured using intense white illumination to enhance spray visualization. Optical diagnostics of flashing sprays continue to pose significant challenges, particularly in distinguishing the liquid phase from the vapor [39]. Since the experimental technique used in this analysis does not incorporate phase-specific imaging post-processing, it is plausible that both liquid and vapor phases are captured concurrently. The comparison with simulation results employs two widely-used spray visualization techniques: Projected Liquid Volume (PLV) and Schlieren, since no simulation post-processing method exists for direct comparison.

First, a comparison with the spray's Projected Liquid Volume [40,41], defined as the projection on a plane of the liquid volume fraction, is provided. The projected plane is the symmetry plane of the spray and, to ensure PLV independency from local mesh refinement regions, the simulation results were first resampled onto a uniform mesh with a grid size of 0.8 mm. Second, the simulation outputs are displayed as two-dimensional slices showing density gradient magnitude. This visualization approach is routinely used to validate numerical models against Schlieren photography [42]. This dual-comparison framework enables a preliminary qualitative examination of spray evolution, capturing both liquid and vapor phase development.

The analysis reveals a dense liquid core extending approximately 100 mm from the nozzle exit, characterized by intense illumination, followed by progressive liquid phase extinction. At approximately 170 mm downstream, most of the liquid has evaporated, as demonstrated by the diminished intensity observed in the PLV and Schlieren visualizations as well as in the experimental photograph. Comparing the PLV and Schlieren distributions in this region shows that the liquid phase concentrates near the spray axis, while the Schlieren exhibits more uniform radial distribution, similar to the experimental image. This observation confirms that the experimental imaging captures light interactions with both liquid and vapor phases.

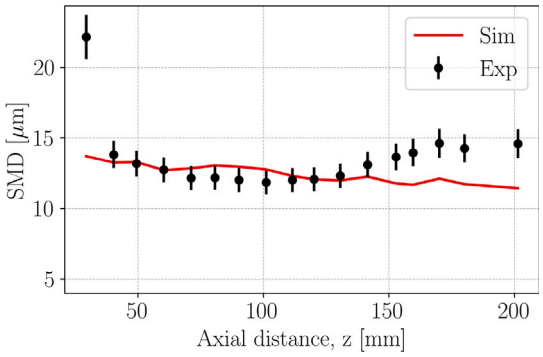

Fig. 5. Variation of SMD of center-line droplets along the spray distance.

Since the simulated condition is in the fully flashing break-up region, the characteristic time of bubble nucleation, growth and burst is faster than the aerodynamic instabilities. Hence, flash boiling starts immediately at the nozzle exit, causing a generalized reduction of the droplet diameter, as represented by the evolution of center-line Sauter Mean Diameter (SMD) in Fig. 5. The centerline computed Sauter mean diameter drops to a value below 20 μm immediately after the exit from the nozzle. The diameter prediction is overall very close to the experimental data. Close to the nozzle, in the dense region, the experimental measurements show a peak in droplet diameter, probably due to some liquid structures that have not been atomized yet. An increase in the droplets' mean diameter is present close to the end of the spray. This can be explained by the random perturbations in the break-up process, producing larger droplets that remain in the environment for a longer time. Droplet coalecescence can be another reason for the discrepancy. Both these aspects will be investigated in a future work.

The sensitivity of the flashing breakup model to the initial droplet size parameter was investigated by testing three initial droplet SMDs ($SMD_0 = 0.25d_N, 0.5d_N, 0.75d_N$). This analysis aimed to assess the response of the atomization model to the injection parameter that typically carries the highest uncertainty. The results, presented in terms of closed nozzle SMD evolution in Fig. 6, show only small relative differences in the post-breakup droplets mean diameter, indicating a limited sensitivity of the model to this parameter. This behavior can be explained by examining the breakup criterion and the formulation of the post-breakup SMD (Eqs. (9) and (10)), which both depend primarily on the thickness of the liquid film constraining the growing vapor bubble, rather than directly on the droplet diameter. Consequently, the initial droplet size mainly affects the characteristic breakup time, larger droplets require a longer time for the vapor bubble to grow until the liquid film becomes unstable, while exerting only a minor influence on the post-breakup droplet diameter. The trend shown in Fig. 6 supports this interpretation, as larger injected droplets exhibit slower breakup. From a physical standpoint, these results underscore the robustness of a thermodynamically based flash-boiling breakup model and highlight its advantage over aerodynamic breakup formulations. In the latter case, since aerodynamic instabilities depend directly on the Weber number, changes in the initial droplet diameter would significantly affect the predicted breakup behavior [43]. Furthermore, the flashing break-up occurs within the first two millimetres from the nozzle, immediately leading to a reduction in the Weber number and inhibiting aerodynamic break-up, as expected for a fully flashing regime.

Flash boiling also affects the thermal evolution of the spray. Since flash-boiling occurs in the near-nozzle region, the vaporization rate is here at its maximum, consistently with the droplet super-heat degree and the corresponding liquid temperature drop. Moving further from the nozzle, the temperature reduction continues until the saturation condition is reached. The left side of Fig. 7 renders the thermophysical evolution of the system in this region, while the droplet temperature evolution along the axis is shown in Fig. 8.

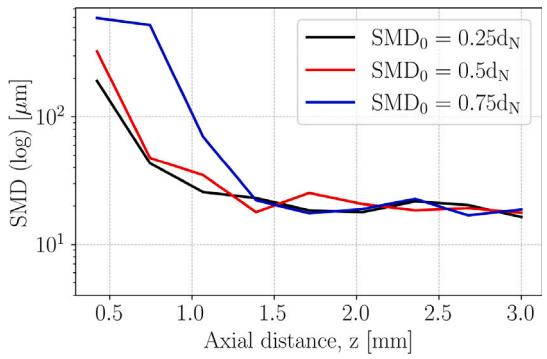

Fig. 6. Variation of SMD of center-line droplets along the spray distance for different droplet initial diameter in the close nozzle region (semi-logarithmic scale).

The temperature tends to decrease along the axis till the saturation point of R134a is reached, which is assessed to be −57.6 °C, according to the thermophysical properties used in this analysis. The vaporization mechanism of superheated liquids is responsible for this type of evolution and it is mainly governed by the difference between liquid vapor and ambient pressures. To ensure energy conservation, the droplet evaporates reducing its temperature T_l and the process stops once $T_l = T_{sat}$. The numerical cooling rate shows a slightly slower trend compared to the experimental measurements. One of the possible causes of this trend may be attributed to the modeling constants employed in the Adachi boiling model Eq. (13). While this correlation, originally developed for pentane sprays and based on the absolute superheat degree, it is widely and successfully applied to describe a variety of flashing sprays. However, its accuracy may vary for fluids with thermophysical properties that differ substantially from the reference fluid [44]. Nevertheless, since the average relative error is 9.3% across the sampling points and the liquid temperature converges toward the expected saturation value, the modeling methodology shows a satisfactory agreement, particularly considering the inherent uncertainties associated with temperature measurements in multiphase flows.

Fig. 9 compares the evolution of the temperature along the radial direction at four different axial locations. The comparison between the experimental measurement and the simulation result is not straightforward. The temperature is measured by a thermocouple, hence, both the liquid and the vapor phases contribute to this estimation. Moreover, the liquid droplets interact differently from the gaseous phase with the thermocouples, both for the differences in thermal conductivity and the possibility of the deposition of a liquid film on the thermocouple.

Since it is difficult to post-process the weight between the contribution of the liquid and vapor, the simulation results in Fig. 9 are presented for both the liquid and the gaseous phases. Experimental results show an initial decrease in temperature along the radial direction, followed by an increase as the distance from the spray axis grows. This behavior can be attributed to the decreasing liquid fraction, which eventually gives way to a region dominated by air. Once the air fraction becomes predominant, the temperature begins to rise. Near the spray axis, the measured temperature closely matches that of the liquid phase. As the distance increases, the temperature gradually diverges from the liquid value and approaches that of the vapor phase.

The evolution of the axial velocity along the radial distance at four different axial positions is presented in Fig. 10. The axial velocity, which is the main component, monotonically decreases along the spray axis due to the aerodynamic drag acting on the droplet. The velocity decreases with the radius, since the periphery of the spray is characterized by a gaseous phase with lower velocity. The simulation describes well the axial velocity profile, which is strictly related to the droplet momentum, a correct prediction of the velocity is hence possible only if the break-up and the evaporation are correctly simulated.

It is interesting to compare the simulation set-up of the present work to the one used in a similar numerical analysis performed on the same experimental apparatus with slightly different liquid (R404A) and injection conditions [45]. The main difference between the two works is the introduction of the flashing break-up model. Since the authors could rely only on the aerodynamic break-up model, they had to impose an initial droplet diameter equal to 9 μm, which is of the same order of magnitude as the droplet after the flashing break-up. The introduction of the flashing break-up model allowed us to impose an initial value equal to half the nozzle diameter. This shows the importance of modeling this phenomenon to correctly predict the spray evolution without imposing artificially small initial diameters.

5.2. Sensitivity analysis

This section describes the results of the sensitivity analysis. Four different thermodynamic conditions are simulated, moving from an injection temperature slightly above saturation conditions (T_{inj} = 250 K) to the validation conditions (T_{inj} = 300 K). The increase of ambient temperature and the corresponding saturation pressure reduces the flash boiling break-up time with respect to the aerodynamic one.

Fig. 11 represents the spray morphology and the droplets' diameter of the analyzed cases. At the lower conditions (ΦJa = 5), the superheat degree is insufficient to trigger the bubble nucleation inside the droplets, hence the dominant break-up mechanism is the mechanical break-up. Since this injection condition is characterized by a large nozzle diameter and relatively low injection pressure, the intensity of this type of break-up is limited. From the second simulated case (ΦJa = 22), the thermodynamic conditions of the droplet are metastable enough to trigger the flash boiling break-up mechanism, resulting in a drastic drop of the droplet diameter. From the mathematical point of view, this behavior is related to the dependency of the initial bubble radius (Eq. (5)) and the bubble growth rate (Eq. (6)) on the superheat degree, expressed difference between the saturation pressure at ambient temperature and the ambient pressure. A further evolution of the break-up regime is visible in the validation conditions (ΦJa = 122), representing the case with the highest possible superheat degree, since the liquid is saturated at injection pressure. This condition shows a further reduction of the characteristic time of flash boiling atomization, moving the break-up closer to the nozzle. A stronger reduction of the final droplets' diameter is also found. To quantify these differences, the Sauter mean diameter *smd* at steady-state conditions of the different cases is reported in Table 2. The *smd* deriving from the mechanical break-up is one order of magnitude larger than the one from flash boiling. Moreover, the validation case shows a further reduction of the diameter, decreasing from 35.7 μm for the case at (ΦJa = 43) to 13.7 μm. The morphology of the spray is a consequence of the break-up regime. The mechanically driven break-up is limited, hence the droplets are characterized by a larger momentum, since the break-up does not affect the droplet velocity. Therefore, they tend to preserve the original injection direction. The stronger the flash boiling, the smaller the particles and the earlier the break-up occurs. For the validation case, the intensity is strong enough to alter the spray morphology, with the mechanism described in Section 5.1. According to the classification proposed by Cleary [11], the first case (ΦJa = 5) is in the mechanical break-up regime. ΦJa = 22 and ΦJa = 43 can be classified in the transient regime, since flash boiling occurs but does not alter significantly the spray morphology. Finally, the validation case is fully flashing, since the flash boiling break-up significantly affects the spray evolution. These results are achieved without any tuning of the simulation set-up. Hence, the proposed numerical model is sensitive to the Jakob number of the specific spray condition.

The break-up regime also has a relevant effect on the thermal state of both the vapor and liquid phases, since the evaporation rate

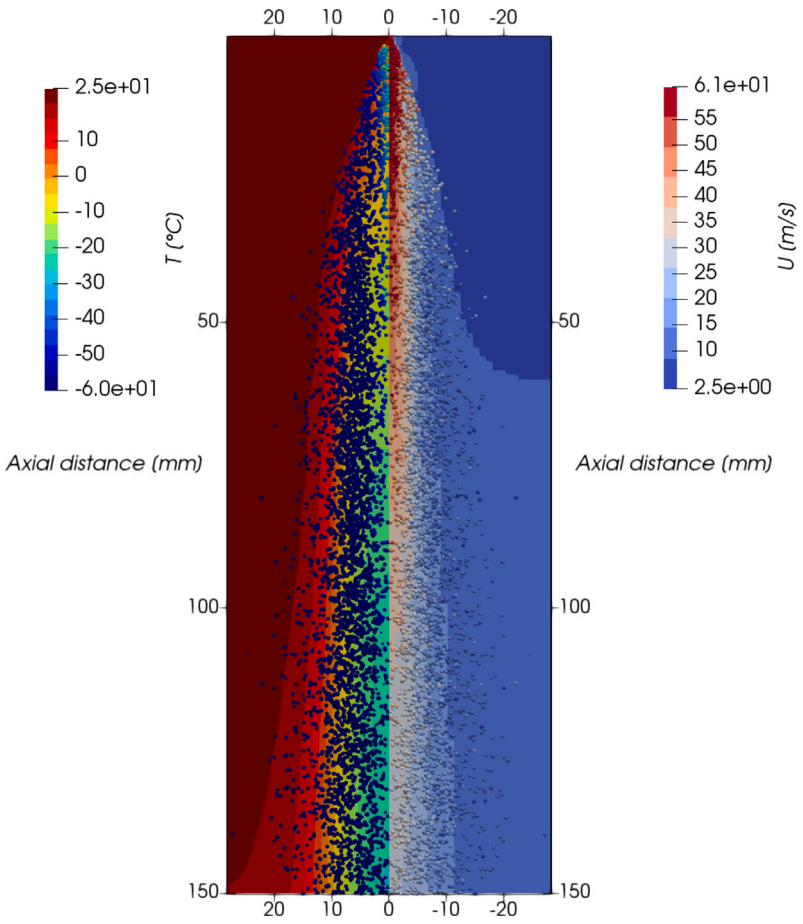

Fig. 7. Graphical rendering of the near-nozzle spray region (up to 150 mm from the injector). Left: droplet temperature superimposed on the gaseous phase temperature field. Right: droplet velocity superimposed on the gaseous phase velocity field.

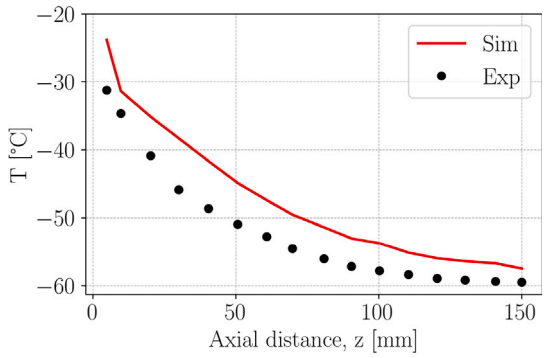

Fig. 8. Variation of temperature of center-line droplets along the spray distance.

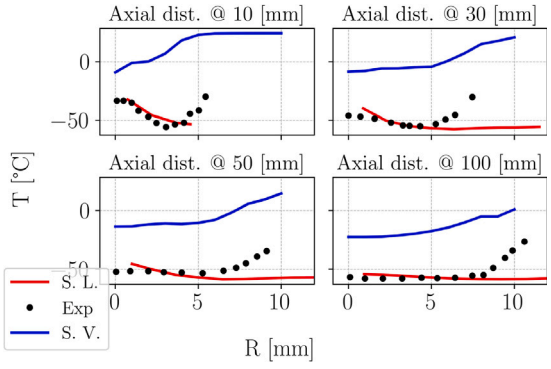

Fig. 9. Radial temperature distributions at four spray distances. Red and blue lines represent simulated liquid and vapor temperatures, respectively; black markers represent experimental measurements.

Table 2
Spray parameters at steady-state conditions.

ΦJa	smd [μm]	$m_{R134a,vapor}$ [kg]	T [K]
5	252.17	1.20e−05	296.381
22	37.60	4.32e−05	287.43
43	35.89	4.24e−05	287.43
121	13.7	5.8e−05	281.06

is proportional to the superheat degree (Eq. (13)). Fig. 12 shows the mass fraction of R134a and the temperature of the vapor phase for the different simulations. The mechanical break-up case shows a small evaporation, since the driving force is classic boiling. The vapor temperature is therefore close to the ambient one, since the boiling evaporation is relatively slow and the droplets are large. The cases dominated by flash-boiling show a consistent evaporation, which leads to a cooling of the vapor phase. The temperature difference between the transient and the fully developed regime is in the order of 40 °C in the core of the spray, marking the differences between the transient

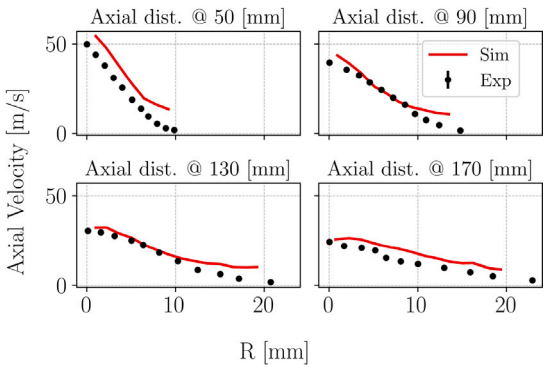

Fig. 10. Variation of axial velocity along the radial direction at four spray distances.

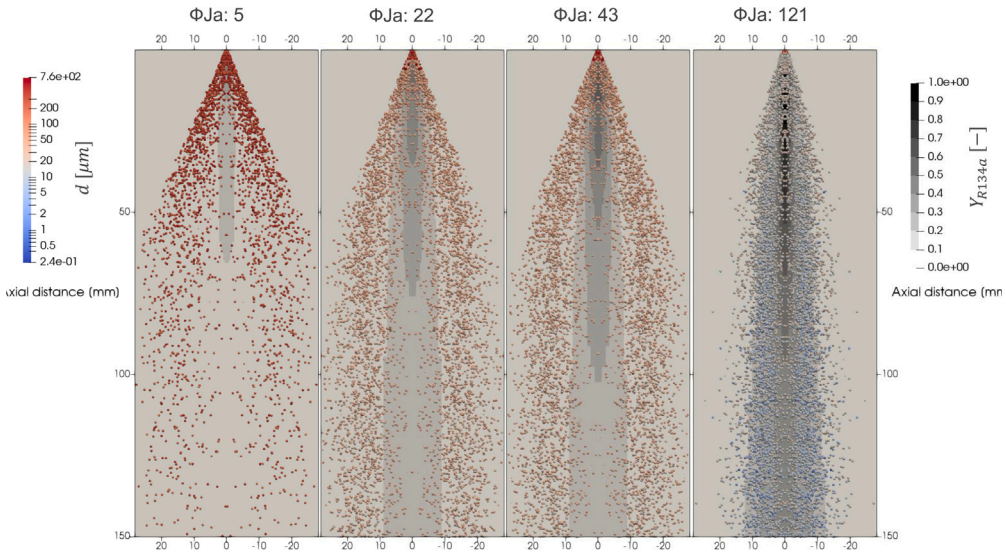

Fig. 11. Spray morphology varying Jakob number, background field is the mass fraction of R134a, Lagrangian point colored by droplet diameter.

and the fully flashing regimes. Table 2 reports the mass of gaseous R134a present in the domain (computed as the domain integral of the product between the density and the R134a mass fraction), as well as the average domain temperature at steady state conditions. Both quantities directly reflect the droplets' evaporation rate and therefore provide a quantitative measure of the flash boiling intensity. Fig. 13 represents the average droplet temperature for the four conditions, sampled along the spray axis. Since all the conditions are super-heated, the droplets tend to cool down to reach the saturated conditions at ambient pressure. The cooling velocity differs among the break-up regimes. The case at ΦJa = 5 reaches this condition slowly; the transient and fully-developed cases otherwise have a much faster cooling rate.

6. Conclusions

This work proposes the application of a CFD approach developed in the Eulerian–Lagrangian framework to accurately simulate cryogenic sprays. The main novelty of the methodology consists in considering the break-up as triggered by two mechanisms. Indeed, the standard aerodynamic-driven break-up mechanism works alongside a flash boiling break-up model. A specific model for the phase transition of a liquid in super-heated conditions was used.

The cryogenic injection of R134a was validated against an experiment carried on by Zhou et al. [45]. The overall spray morphology and the evolution of the droplets' thermophysical properties are in good agreement with the experimental findings. The main results obtained from the simulation are:

- The flash boiling break-up model accurately captures the atomization process, which occurs near the nozzle, characteristic of a fully flashing regime, and produces a highly atomized spray. As a result, the model provides a reliable prediction of the average droplet diameter along the spray axis.
- Super-heated phase change phenomenology is correctly captured by the simulation, since a decrease of the droplet temperature tending to the saturation temperature at ambient pressure is observed.
- The evolution of spray velocity along the radial direction at various axial positions demonstrates that the spray morphology and the far-field spray angle are accurately reproduced. This indicates that the simulated droplet momentum far from the nozzle is well captured, reflecting the accurate modeling of both breakup and phase change processes.

The sensitivity of the proposed model to the different break-up regimes was tested by varying the injection conditions. Four conditions were considered to cover the fully-flashing, transient and mechanically driven break-up regimes. The model proved to be sensitive to the injection conditions, in particular:

- The breakup model is sensitive to the Jakob number, exhibiting minimal breakup in the mechanically guided regime and transitioning to intense breakup at the nozzle exit under fully flashing conditions, passing through an intermediate regime. As a result, the spray morphology differs between cases: in the mechanical

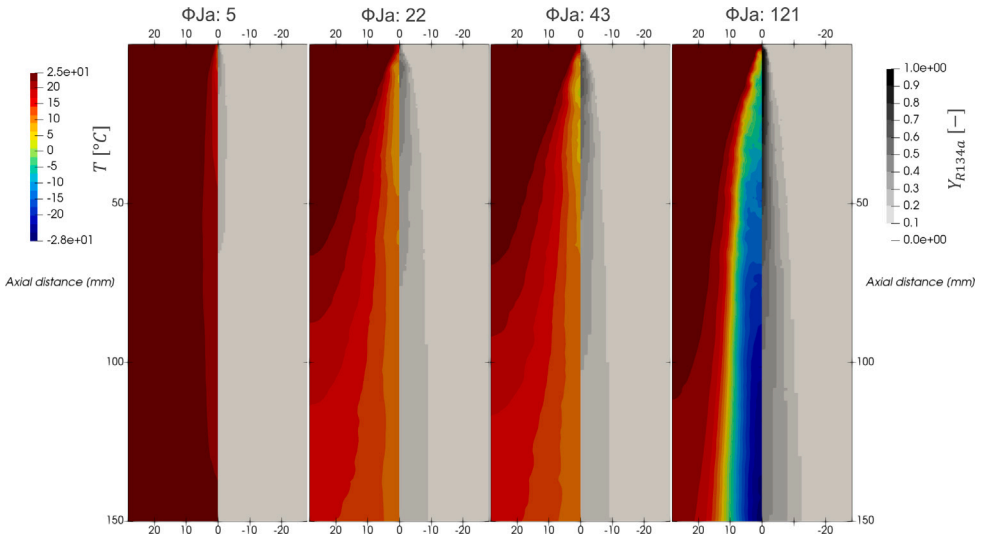

Fig. 12. Vapor temperature and R134 mass fraction fields varying Jakob number.

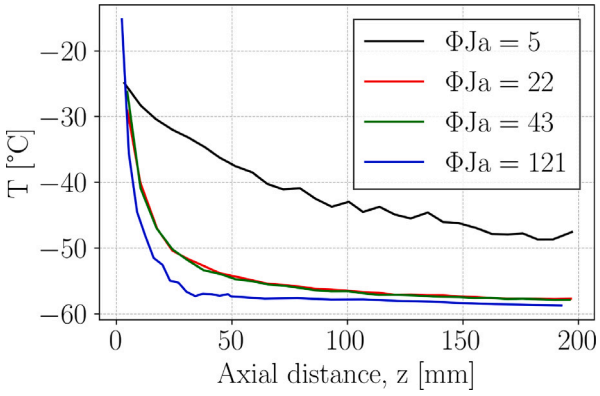

Fig. 13. Average droplet temperature along spray axis varying Jakob number.

breakup regime, droplets tend to maintain the original spray angle, whereas in the fully flashing regime, a noticeable spray collapse occurs;

- The phase change model is also sensitive to the spray regime: the greater the degree of superheat, the more energy is retained within the droplets, leading to a more intense phase change. As a result, spray-induced cooling of the surrounding air is minimal in the mechanical regime but becomes significant under fully flashing conditions. This phenomenon also affects the droplet cooling rate, which increases with the degree of superheat.

It is important to note that the use of the flashing atomization model allows one to achieve the results presented without tuning the initial diameters of the droplets, as was necessary for other authors working on a similar experimental case [45].

CRediT authorship contribution statement

Mattia Pelosin: Writing – review & editing, Writing – original draft, Software, Methodology, Investigation, Formal analysis, Data curation, Conceptualization. **Francesco Duronio:** Writing – review & editing, Methodology. **Paolo Albertelli:** Supervision, Conceptualization. **Tommaso Lucchini:** Writing – review & editing, Supervision, Conceptualization. **Zhifu Zhou:** Validation, Supervision. **Jiameng Tian:** Writing – review & editing, Validation. **Bin Chen:** Writing – review & editing, Validation.

Funding

The work of Francesco Duronio has been funded by the European Union - NextGenerationEU, Mission 4, Component 1, under the Italian Ministry of University and Research (MUR) National Innovation Ecosystem grant ECS00000041 - VITALITY - CUP E13C22001060006.

Declaration of competing interest

The authors declare that they have no known competing financial interests or personal relationships that could have appeared to influence the work reported in this paper.

Data availability

The authors do not have permission to share data.

References

[1] Michael L. Meyer, David J. Chato, David W. Plachta, Gregory A. Zimmerli, Stephen J. Barsi, Neil T. Van Dresar, Jeffrey P. Moder, Mastering cryogenic propellants, J. Aerosp. Eng. 26 (2) (2013) 343–351, http://dx.doi.org/10.1061/(ASCE)AS.1943-5525.0000297, URL https://www.scopus.com/inward/record.uri?eid=2-s2.0-84879206583&doi=10.1061%2f%28ASCE%29AS.1943-5525.0000297&partnerID=40&md5=7f3425550e9ddc32a58d23b3c95090d5. Cited by: 25; All Open Access, Green Open Access.

[2] A. Shokrani, V. Dhokia, P. Muñoz-Escalona, S.T. Newman, State-of-the-art cryogenic machining and processing, Int. J. Comput. Integr. Manuf. 26 (7) (2013) 616–648, http://dx.doi.org/10.1080/0951192X.2012.749531.

[3] J. Stuart Nelson, Thomas E. Milner, Bahman Anvari, B. Samuel Tanenbaum, Sol Kimel, Lars O. Svaasand, Steven L. Jacques, Dynamic epidermal cooling during pulsed laser treatment of port-wine stain: A new methodology with preliminary clinical evaluation, Arch. Dermatol. (ISSN: 0003-987X) 131 (6) (1995) 695–700, http://dx.doi.org/10.1001/archderm.1995.01690180071013.

[4] Bharat Bhatia, Ashoke De, Flash boiling in sprays: Recent developments and modeling, J. Indian Inst. Sci. (ISSN: 0019-4964) 99 (1) (2019) 93–104, http://dx.doi.org/10.1007/s41745-019-0104-x.

[5] Eran Sher, Tali Bar-Kohany, Alexander Rashkovan, Flash-boiling atomization, Prog. Energy Combust. Sci. (ISSN: 0360-1285) 34 (4) (2008) 417–439, http://dx.doi.org/10.1016/j.pecs.2007.05.001, URL https://www.sciencedirect.com/science/article/pii/S0360128507000500.

[6] Mengzhao Chang, Ziyoung Lee, Sungwook Park, Suhan Park, Characteristics of flash boiling and its effects on spray behavior in gasoline direct injection injectors: A review, Fuel (ISSN: 0016-2361) 271 (2020) 117600, http://dx.doi.org/10.1016/j.fuel.2020.117600, URL https://www.sciencedirect.com/science/article/pii/S0016236120305950.

[7] ZhiWei Zhang, DingHua Hu, Qiang Li, Chao Liu, Fan Zhou, Visualization study on atomization characteristics and heat transfer performance of R1336mzz flash spray cooling, Sci. China Technol. Sci. (ISSN: 1869-1900) 64 (10) (2021) 2099–2109, http://dx.doi.org/10.1007/s11431-021-1853-4.

[8] Min Xu, Yuyin Zhang, Wei Zeng, Gaoming Zhang, Ming Zhang, Flash boiling: Easy and better way to generate ideal sprays than the high injection pressure, SAE Int. J. Fuels Lubr. 6 (2013) 137–148, http://dx.doi.org/10.4271/2013-01-1614.

[9] R.D. Oza, On the mechanism of flashing injection of initially subcooled fuels, J. Fluids Eng. (ISSN: 0098-2202) 106 (1) (1984) 105–109, http://dx.doi.org/10.1115/1.3242383.

[10] Byung Suh Park, Sang Yong Lee, An experimental investigation of the flash atomization mechanism, At. Sprays 4 (2) (1994).

[11] Vincent Cleary, Phil Bowen, Henk Witlox, Flashing liquid jets and two-phase droplet dispersion: I. Experiments for derivation of droplet atomisation correlations, J. Hazard. Mater. (ISSN: 0304-3894) 142 (3) (2007) 786–796, http://dx.doi.org/10.1016/j.jhazmat.2006.06.125, URL https://www.sciencedirect.com/science/article/pii/S0304389406007424. Papers Presented at the 2005 Symposium of the Mary Kay O'Connor Process Safety Center.

[12] Chinmoy K Mohapatra, David P Schmidt, Brandon A Sforzo, Katarzyna E Matusik, Zongyu Yue, Christopher F Powell, Sibendu Som, Balaji Mohan, Hong G Im, Jihad Badra, Mathis Bode, Heinz Pitsch, Dimitrios Papoulias, Kshitij Neroorkar, Samir Muzaferija, Pedro Martí-Aldaraví, María Martínez, Collaborative investigation of the internal flow and near-nozzle flow of an eight-hole gasoline injector (Engine Combustion Network Spray G), Int. J. Engine Res. 24 (6) (2023) 2297–2314, http://dx.doi.org/10.1177/14680874209184449, URL https://www.scopus.com/inward/record.uri?eid=2-s2.0-85086339081&doi=10.1177%2f14680874209184449&partnerID=40&md5=1fedb50094982ed3a452a30b0c4cf34c. Cited by: 35; All Open Access, Green Open Access.

[13] Brandon A. Sforzo, Aniket Tekawade, Alan L. Kastengren, Kamel Fezzaa, Jan Ilavsky, Christopher F. Powell, Yuanjiang Pei, Anqi Zhang, Robert Levy, X-Ray characterization of real fuel sprays for gasoline direct injection, J. Energy Resour. Technol. Trans. the ASME 144 (2) (2022) http://dx.doi.org/10.1115/1.4050979, URL https://www.scopus.com/inward/record.uri?eid=2-s2.0-85127379853&doi=10.1115%2f1.4050979&partnerID=40&md5=1b3881776cabf180cd2ba46308f7c003. Cited by: 10; All Open Access, Green Open Access.

[14] Maryam Moulai, Ronald Grover, Scott Parrish, David Schmidt, Internal and near-nozzle flow in a multi-hole gasoline injector under flashing and non-flashing conditions, SAE Tech. Pap. Ser. 1 (2015) http://dx.doi.org/10.4271/2015-01-0944.

[15] Hengjie Guo, Lorenzo Nocivelli, Roberto Torelli, Numerical study on spray collapse process of ECN spray G injector under flash boiling conditions, Fuel (ISSN: 0016-2361) 290 (2021) 119961, http://dx.doi.org/10.1016/j.fuel.2020.119961, URL https://www.sciencedirect.com/science/article/pii/S0016236120329574.

[16] Francesco Duronio, Andrea Di Mascio, Implementation and assessment of a low-dissipative OpenFOAM solver for compressible multi-species flows, Comput. & Fluids (ISSN: 0045-7930) 274 (2024) 106240, http://dx.doi.org/10.1016/j.compfluid.2024.106240, URL https://www.sciencedirect.com/science/article/pii/S0045793024000720.

[17] Mark A. Patterson, Rolf D. Reitz, Modeling the effects of fuel spray characteristics on diesel engine combustion and emission, Journal Engines 3 (1998) 19, http://dx.doi.org/10.4271/980131.

[18] Rolf Reitz, Ramachandra Diwakar, Effect of drop breakup on fuel sprays, SAE Trans. 95 (1986) 218–227, http://dx.doi.org/10.4271/860469, URL https://api.semanticscholar.org/CorpusID:93006775.

[19] J. Zembi, M. Battistoni, A. Pandal, R. Pelé, P. Brequigny, C. Hespel, C. Mounaïm-Rousselle, Lagrangian CFD modeling of ammonia sprays: A correlation across flash boiling and evaporative conditions, Int. Commun. Heat Mass Transfer (ISSN: 0735-1933) 158 (2024) 107866, http://dx.doi.org/10.1016/j.icheatmasstransfer.2024.107866, URL https://www.sciencedirect.com/science/article/pii/S0735193324006286.

[20] Rui Wang, Bin Chen, Xin-Sheng Wang, Numerical simulation of cryogen spray cooling by a three-dimensional hybrid vortex method, Appl. Therm. Eng. (ISSN: 1359-4311) 119 (2017) 319–330, http://dx.doi.org/10.1016/j.applthermaleng.2017.03.066, URL https://www.sciencedirect.com/science/article/pii/S1359431116337206.

[21] Francesco Duronio, Andrea Di Mascio, Carlo Villante, Michele Anatone, Angelo De Vita, ECN Spray G: Coupled Eulerian internal nozzle flow and Lagrangian spray simulation in flash boiling conditions, Int. J. Engine Res. 14680874221090732, http://dx.doi.org/10.1177/14680874221090732.

[22] Avijit Saha, Temistocle Grenga, Abhishek Y. Deshmukh, Jörn Hinrichs, Mathis Bode, Heinz Pitsch, Numerical modeling of single droplet flash boiling behavior of e-fuels considering internal and external vaporization, Fuel (ISSN: 0016-2361) 308 (2022) 121934, http://dx.doi.org/10.1016/j.fuel.2021.121934, URL https://www.sciencedirect.com/science/article/pii/S0016236121018111.

[23] Jan Breitenbach, Ilia V. Roisman, Cameron Tropea, Heat transfer in the film boiling regime: Single drop impact and spray cooling, Int. J. Heat Mass Transfer (ISSN: 00179310) 110 (2017) 34–42, http://dx.doi.org/10.1016/j.ijheatmasstransfer.2017.03.004.

[24] Chengxin Bai, A.D. Gosman, Development of methodology for spray impingement simulation, SAE Tech. Pap. (ISSN: 26883627) (1995) 550–568, http://dx.doi.org/10.4271/950283.

[25] Henk W.M. Witlox, Mike Harper, Adeyemi Oke, Philip J. Bowen, Peter Kay, Sub-cooled and flashing liquid jets and droplet dispersion I. Overview and model implementation/validation, J. Loss Prev. Process. Ind. (ISSN: 0950-4230) 23 (6) (2010) 831–842, http://dx.doi.org/10.1016/j.jlp.2010.07.004, URL https://www.sciencedirect.com/science/article/pii/S0950423010000902. Papers Presented at the 2009 International Symposium of the Mary Kay O'Connor Process Safety Center.

[26] Davide Paredi, Tommaso Lucchini, Gianluca D'Errico, Angelo Onorati, Alessandro Montanaro, Luigi Allocca, Roberto Ianniello, Combined experimental and numerical investigation of the ECN spray G under different engine-like conditions, SAE Tech. Pap. (2018) http://dx.doi.org/10.4271/2018-01-0281.

[27] Zhou Zhifu, Wu Weitao, Chen Bin, Wang Guoxiang, Guo Liejin, An experimental study on the spray and thermal characteristics of R134a two-phase flashing spray, Int. J. Heat Mass Transfer (ISSN: 0017-9310) 55 (15) (2012) 4460–4468, http://dx.doi.org/10.1016/j.ijheatmasstransfer.2012.04.021, URL https://www.sciencedirect.com/science/article/pii/S0017931012002645.

[28] Francesco Duronio, Stefano Ranieri, Alessandro Montanaro, Luigi Allocca, Angelo De Vita, ECN spray G injector: Numerical modelling of flash-boiling breakup and spray collapse, Int. J. Multiph. Flow (ISSN: 0301-9322) 145 (2021) 103817, http://dx.doi.org/10.1016/j.ijmultiphaseflow.2021.103817, URL https://www.sciencedirect.com/science/article/pii/S0301932221002470.

[29] Grazia Lamanna, Hend Kamoun, Bernhard Weigand, Johan Steelant, Towards a unified treatment of fully flashing sprays, Int. J. Multiph. Flow (ISSN: 0301-9322) 58 (2014) 168–184, http://dx.doi.org/10.1016/j.ijmultiphaseflow.2013.08.010, URL https://www.sciencedirect.com/science/article/pii/S0301932213001298.

[30] Marianna Migliaccio, Alessandro Montanaro, Davide Paredi, Tommaso Lucchini, Luigi Allocca, Gianluca D'Errico, CFD Modeling and Validation of the ECN Spray G Experiment under a Wide Range of Operating Conditions, in: SAE Technical Papers, 2019, p. 13, http://dx.doi.org/10.4271/2019-24-0130.

[31] Davide Paredi, Tommaso Lucchini, Gianluca D'Errico, Angelo Onorati, Lyle Pickett, Joshua Lacey, Validation of a comprehensive computational fluid dynamics methodology to predict the direct injection process of gasoline sprays using Spray G experimental data, Int. J. Engine Res. (ISSN: 20413149) (2020) http://dx.doi.org/10.1177/1468087419868020.

[32] Masayuki Adachi, Vincent G McDonell, Daisuke Tanaka, Jiro Senda, Hajime Fujimoto, Characterization of fuel vapor concentration inside a flash boiling spray, Anal. Engine Combust. Flow Diagnostics-SP-1244 (1997) http://dx.doi.org/10.4271/970871.

[33] Francesco Duronio, Michele Battistoni, Andrea Di Mascio, Angelo De Vita, Faniry Nadia Zazaravaka Rahantamialisoa, Jacopo Zembi, A real-fluid low-dissipative solver for flash boiling simulations of non-equilibrium mixtures, Int. J. Heat Mass Transfer (ISSN: 0017-9310) 225 (2024) 125391, http://dx.doi.org/10.1016/j.ijheatmasstransfer.2024.125391, URL https://www.sciencedirect.com/science/article/pii/S0017931024002229.

[34] M. Pilch, C.A. Erdman, Use of breakup time data and velocity history data to predict the maximum size of stable fragments for acceleration-induced breakup of a liquid drop, Int. J. Multiph. Flow (ISSN: 0301-9322) 13 (6) (1987) 741–757, http://dx.doi.org/10.1016/0301-9322(87)90063-2, URL https://www.sciencedirect.com/science/article/pii/0301932287900632.

[35] B. Zuo, A. Gomes, Christopher Rutland, Modeling superheated fuel spray and vaporization, Int. J. Engine Res. - INT J ENGINE RES 1 (2000) 321–336, http://dx.doi.org/10.1243/1468087001545218, URL https://journals.sagepub.com/doi/10.1243/1468087001545218.

[36] F. Payri, V. Bermúdez, R. Payri, F.J. Salvador, The influence of cavitation on the internal flow and the spray characteristics in diesel injection nozzles, Fuel (ISSN: 0016-2361) 83 (4) (2004) 419–431, http://dx.doi.org/10.1016/j.fuel.2003.09.010, URL https://www.sciencedirect.com/science/article/pii/S0016236103003193.

[37] Rong Xue, Yixiao Ruan, Xiufang Liu, Liang Chen, Xingqun Zhang, Yu Hou, Shuangtao Chen, Experimental study of liquid nitrogen spray characteristics in atmospheric environment, Appl. Therm. Eng. 142 (2018) http://dx.doi.org/10.1016/j.applthermaleng.2018.07.056.

[38] Ian H. Bell, Jorrit Wronski, Sylvain Quoilin, Vincent Lemort, Pure and pseudo-pure fluid thermophysical property evaluation and the open-source thermophysical property library CoolProp, Ind. Eng. Chem. Res. 53 (6) (2014) 2498–2508, http://dx.doi.org/10.1021/ie4033999, URL http://pubs.acs.org/doi/abs/10.1021/ie4033999.

[39] Fahad Almatrafi, Hao Wu, Santiago Cardona, Moez Ben Houidi, William L. Roberts, An analysis of flashing and non-flashing ammonia sprays using DBI, mie scattering, shadowgraphy, and schlieren, Exp. Fluids (ISSN: 1432-1114) 66 (10) (2025) 196, http://dx.doi.org/10.1007/s00348-025-04126-6.

[40] Joonsik Hwang, Lukas Weiss, Ioannis K. Karathanassis, Phoevos Koukouvinis, Lyle M. Pickett, Scott A. Skeen, Spatio-temporal identification of plume dynamics by 3D computed tomography using engine combustion network spray G injector and various fuels, Fuel (ISSN: 0016-2361) 280 (2020) 118359, http://dx.doi.org/10.1016/j.fuel.2020.118359, URL https://www.sciencedirect.com/science/article/pii/S0016236120313557.

[41] Fabien Tagliante, Tuan M. Nguyen, Lyle M. Pickett, Hyung Sub Sim, Large-eddy simulation of laser-ignited direct injection gasoline spray for emission control, Energies (ISSN: 1996-1073) 14 (21) (2021) http://dx.doi.org/10.3390/en14217276, URL https://www.mdpi.com/1996-1073/14/21/7276.

[42] Maurizio Lazzaro, Characterization of the liquid phase of vaporizing GDI sprays from schlieren imaging, Meas. Sci. Technol. 30 (8) (2019) 085401, http://dx.doi.org/10.1088/1361-6501/ab228d.

[43] Filippo Gerbino, Giovanni Tretola, Robert Morgan, Penny Atkins, Konstantina Vogiatzaki, Influence of the initial droplet distribution on the prediction of spray dynamics in Eulerian-Lagrangian simulations, Int. J. Multiph. Flow (ISSN: 0301-9322) 141 (2021) 103642, http://dx.doi.org/10.1016/j.ijmultiphaseflow.2021.103642, URL https://www.sciencedirect.com/science/article/pii/S0301932221000902.

[44] Thomas Ramcke, Arne Lampmann, Michael Pfitzner, Simulations of injection of liquid oxygen/gaseous methane under flashing conditions, J. Propuls. Power 34 (2017) 1–13, http://dx.doi.org/10.2514/1.B36412.

[45] Zhi-Fu Zhou, Guan-Yu Lu, Bin Chen, Numerical study on the spray and thermal characteristics of R404A flashing spray using OpenFOAM, Int. J. Heat Mass Transfer (ISSN: 0017-9310) 117 (2018) 1312–1321, http://dx.doi.org/10.1016/j.ijheatmasstransfer.2017.10.095, URL https://www.sciencedirect.com/science/article/pii/S0017931017330958.